Chaotic dynamics in miniband semiconductor superlattices under crossed electric and magnetic fields

C. Wang and J. C. Cao*

State Key Laboratory of Functional Materials for Informatics, Shanghai Institute of Microsystem and Information Technology, Chinese Academy of Sciences and Graduate School of Chinese Academy of Sciences, 865 Changning Road, Shanghai 200050, People's Republic of China

(Received 28 January 2005; revised manuscript received 27 April 2005; published 18 July 2005)

We have theoretically studied chaotic dynamics of ballistic electrons in a GaAs-based miniband semiconductor superlattice with a terahertz electric field parallel to and a magnetic field perpendicular to the growth axis, using the semiclassical balance equation model with elastic and inelastic scattering. The effect of magnetic field is included in the balance equations which incorporate the self-consistent electric field. The electron motion within the miniband superlattice produces a cooperative nonlinear oscillatory mode with the influence of self-consistent electric field and magnetic field. Complicated chaotic dynamical characteristics show up with the external electric field driving amplitude, driving frequency, and magnetic field as the control parameters. The temporal behaviors of the nonlinear dynamical system are analyzed with different techniques, such as Lyapunov exponent, Poincaré bifurcation diagram, phase plot, first return map, and power spectrum.

DOI: 10.1103/PhysRevB.72.045339 PACS number(s): 73.61.Ey, 73.50.Fq, 85.30.Fg, 85.30.De

I. INTRODUCTION

Since the study of Esaki and Tsu,[1] there has been a great deal of theoretical and experimental work about electron transport in semiconductor superlattices driven by an intense terahertz (THz) electric field in the literature.[2–25] Under the influence of an external THz electric field, semiconductor superlattices exhibit many interesting phenomena including multistable phenomena,[6] dc-current suppression,[7] multiphoton assisted resonant tunneling,[8] negative absolute resistance,[9] Shapiro steps on dc current-voltage curve,[10,11] and abundant harmonic generation.[12] In the past several years, chaotic dynamics in semiconductor superlattices has been the subject of growing interest. Bulashenko *et al.*[13] first predicted the appearance of chaotic behaviors in sequential resonant tunneling superlattice by applying a small ac signal to the dc-biased self-oscillating system.[14] The bifurcation scenario to chaos and the transition between synchronization and chaos have also been further studied experimentally in an incommensurate sinusoidal voltage driven superlattice system.[15–17] When a miniband superlattice is subject to a dc+ac electric field, the superlattice system can also produce an alternative mode of operation and various types of chaos,[20] which is due to the spatiotemporal electric field domain induced space charge instability. Recently, ballistic electron motion in the miniband of semiconductor superlattice[21,22] and quantum-dot superlattice[24] with the influence of an intense THz electric field has been studied using the semiclassical balance equation approach. It is shown that the collective effects (via a self-consistent field) on the electron's motion can lead to the appearance of dissipative chaos.

Electron transport in doped or undoped superlattice under electric and magnetic fields[26–30] has also been studied theoretically and experimentally. In semiconductor superlattices with a magnetic field perpendicular to the growth axis, the current peak of the current-voltage characteristic shifts to a larger electric field because the magnetic field impedes the increase of momentum along the growth axis.[26,27] Magneto-suppression of the superlattice miniband conduction has been observed in undoped miniband superlattice system with a strong magnetic field applied parallel to the growth axis. It is shown that the suppression originates from the decrease of carrier injection rate from the heavily doped emitter into the superlattice layers with the increase of magnetic field.[28] Schmidt *et al.*[29] investigated the formation of electric field domains, which remains determined by the subband spacing rather than by the cyclotron energy, in Landau-quantized superlattices by applying magnetic fields up to 29 T. Moreover, chaotic electron transport has been investigated with a tilted magnetic field applied to the miniband superlattice, which is considered to be a non-Kolmogorov-Arnol'd-Moser system and experimentally accessible.[30]

In this paper, we study the chaotic dynamics of ballistic electron transport in the lowest miniband of semiconductor superlattices with an intense THz electric field parallel to and a magnetic field perpendicular to the growth axis, using a set of phenomenological balance equations including the influence of the self-consistent electric field. Numerical simulations indicate that different time-dependent solutions of electron velocity show up, including periodic, quasiperiodic, and chaotic solutions. These complicated nonlinear solutions can be controlled by the ac electric field amplitude, ac frequency, and magnetic field. We carry out a detailed analysis of the solutions with different chaos-detecting techniques. The remainder of this paper is organized as follows. In Sec. II, we describe the semiclassical balance equation approach, which incorporates the influence of self-consistent electric field generated by electron motion and magnetic field. In Sec. III, the temporal evolution of average electron velocities are simulated for different magnetic fields with a set of experimental parameters. The chaotic dynamical properties of electron transport are studied in detail with ac amplitude, ac frequency, and magnetic field as control parameters in Sec. IV. Different chaos-detecting techniques including Lyapunov exponent, phase plot, first return map, and power spectrum are introduced in this section. In Sec. V, we draw the main conclusions of the work.

II. BALANCE EQUATIONS FOR ELECTRON TRANSPORT IN THE MINIBAND OF SUPERLATTICES

We consider the motion of ballistic electron through the lowest miniband of spatially homogeneous GaAs-based semiconductor superlattices along the growth axis (the z direction). For electrons confined to the single miniband, the energy-wave-vector dispersion relation for the miniband within the tight-binding approximation is

$$\varepsilon(\mathbf{k}) = \frac{\Delta}{2}[1-\cos(k_z a)] + \hbar^2(k_x^2+k_y^2)/2m^*, \tag{1}$$

in which Δ is the miniband width, $\mathbf{k}=(k_x,k_y,k_z)$ is the wave vector, a is the period of the superlattice, m^* is the effective mass within the x-y plane of quantum wells, and $\hbar$ is the Planck constant. When an external electric field with the amplitude E_Ω and frequency Ω in the form $E_{\rm ext}(t)=E_\Omega\cos(\Omega t)$ is applied in the z direction, the total electric field acts on electrons, $E_{\rm tot}(t)$ is the sum of the external field $E_{\rm ext}(t)$ and the self-consistent field $E_{\rm sc}(t)$,[22] i.e.,

$$E_{\rm tot}(t) = E_{\rm sc}(t) + E_{\rm ext}(t). \tag{2}$$

The self-consistent field $E_{\rm sc}(t)$ (Ref. 22) incorporates the influence of the external circuit on the superlattice system and the electron's interaction with other electrons. When a constant magnetic field B is applied parallel to the x axis, the electron is accelerated by the applied electric and magnetic fields according to $\dot{\mathbf{k}}=-(e/\hbar)(\mathbf{E}+\mathbf{V}\times\mathbf{B})$, with electron charge $-e$ and average electron velocity $\mathbf{V}=(V_y,V_z)$. The acceleration of the external fields is balanced by the elastic and inelastic scattering processes which limit the momentum of electrons. Generalizing the balance equation approach of Ref. 2 to include the effect of magnetic field and the self-consistent electric field, we get the equations describing the electron's motion in the miniband of superlattices as follows:[21,22,27]

$$\frac{dV_y}{dt} = -\frac{eBV_z}{m^*} - \Gamma_{Vy}V_y, \tag{3}$$

$$\frac{dV_z}{dt} = -\frac{e[E_{\rm tot}(t)-BV_y]}{m(\varepsilon_z)} - \Gamma_{Vz}V_z, \tag{4}$$

$$\frac{d\varepsilon_z}{dt} = -eE_{\rm tot}(t)V_z + eBV_yV_z - \Gamma_\varepsilon(\varepsilon_z-\varepsilon_{{\rm eq},z}), \tag{5}$$

$$\frac{dE_{\rm sc}(t)}{dt} = \frac{4\pi}{\epsilon_s}eNV_z - \Lambda E_{\rm sc}, \tag{6}$$

in which ε_z is the average energy of motion along the z axis (longitudinal) with equilibrium value $\varepsilon_{{\rm eq},z}$ (resulting from thermal energy and/or external pump),[21] N is the bulk density of carriers, and ϵ_s is the average dielectric constant for the superlattice. Λ is the relaxation frequency of the external circuit and is discussed in Ref. 22. The parameters Γ_{Vy}, Γ_{Vz}, and Γ_ε are the phenomenological elastic and inelastic relaxation constants of the average electron velocity V_y, V_z, and energy ε_z, respectively. Equations (3) and (4) are the basic equations governing the motion of electrons in the presence of external electric and magnetic fields. The relationship between electron's effective mass $m(\varepsilon_z)$ and the energy ε_z is[2]

$$m(\varepsilon_z) = \frac{m_0}{1-2\varepsilon_z/\Delta}, \tag{7}$$

with $m_0=2\hbar^2/(\Delta a^2)$ the electron's effective mass at the bottom of the miniband. Since the effective mass m^* in the x-y plane is a constant, the transverse energy does not enter Eq. (5), which describes the heating (energy increasing by the external electric and magnetic fields) and cooling (i.e., relaxation of energy) of the electron's energy.[21] The temperature dependence of thermal equilibrium energy value $\varepsilon_{{\rm eq},z}$ is in the form[2,21]

$$\varepsilon_{{\rm eq},z}^{(T)} = \frac{\Delta}{2}\left[1-\frac{I_1(\Delta/2k_BT)}{I_0(\Delta/2k_BT)}\right], \tag{8}$$

where I_0 and I_1 are the modified Bessel functions of zeroth and first order, T is the lattice temperature, and k_B is Boltzmann's constant. Equation (6), which takes into account the effect of the external circuit by involving the relaxation frequency Λ, describes the time evolution of self-consistent electric field.

For the convenience of studying our time-varying electric field and constant magnetic field driven superlattice system, we render Eqs. (3)–(6) dimensionless with the scaling factors: $\omega_s=\sqrt{2\pi e^2N\Delta a^2/(\epsilon_s\hbar^2)}$, $t_s=1/\omega_s$, and $E_s=\hbar\omega_s/(ea)$. As is known, the electron plasma oscillation frequency $\omega_{\rm pl}=\sqrt{4\pi e^2N/(\epsilon_s m_0)}$. If m_0 takes the electron effective mass at the bottom of the miniband, the frequency ω_s is formally equal to $\omega_{\rm pl}$.[21] E_s is the electric field scaling factor. The normalized physical quantities are denoted by: velocity $v_y=\sqrt{m_0m^*}aV_y/\hbar$, $v_z=m_0aV_z/\hbar$, magnetic field $\mathcal{B}=eB/(\omega_s\sqrt{m_0m^*})$, time $\tau=t/t_s$, ac frequency $\omega=\Omega/\omega_s$, ac amplitude $E_\omega=E_\Omega/E_s$, energy $w=(\varepsilon_z-\Delta/2)/(\Delta/2)$, equilibrium energy $w_0=(\varepsilon_{{\rm eq},z}-\Delta/2)/(\Delta/2)$, total electric field acting on electrons $E(\tau)=[E_{\rm sc}(\tau)+E_\Omega\cos(\omega\tau)]/E_s$, relaxation rates $\gamma_{Vy}=\Gamma_{Vy}/\omega_s$, $\gamma_{Vz}=\Gamma_{Vz}/\omega_s$, $\gamma_\varepsilon=\Gamma_\varepsilon/\omega_s$, and $\alpha=\Lambda/\omega_s$. Then, we obtain the dimensionless balance equations as follows:

$$\frac{dv_y}{d\tau} = -\mathcal{B}v_z - \gamma_{V_y}v_y, \tag{9}$$

$$\frac{dv_z}{d\tau} = wE(\tau) - w\mathcal{B}v_y - \gamma_{V_z}v_z, \tag{10}$$

$$\frac{dw}{d\tau} = -E(\tau)v_z + \mathcal{B}v_yv_z - \gamma_\varepsilon(w-w_0), \tag{11}$$

$$\frac{dE(\tau)}{d\tau} = v_z - \alpha E(\tau) + f(\tau), \tag{12}$$

where $f(\tau)=\alpha E_\omega\cos(\omega\tau)-E_\omega\omega\sin(\omega\tau)$.

Now, we have got four dimensionless ordinary differential equations (9)–(12), which describe the motion of ballistic electrons in the lowest miniband of the semiconductor superlattices with the influence of a magnetic field B and an ex-

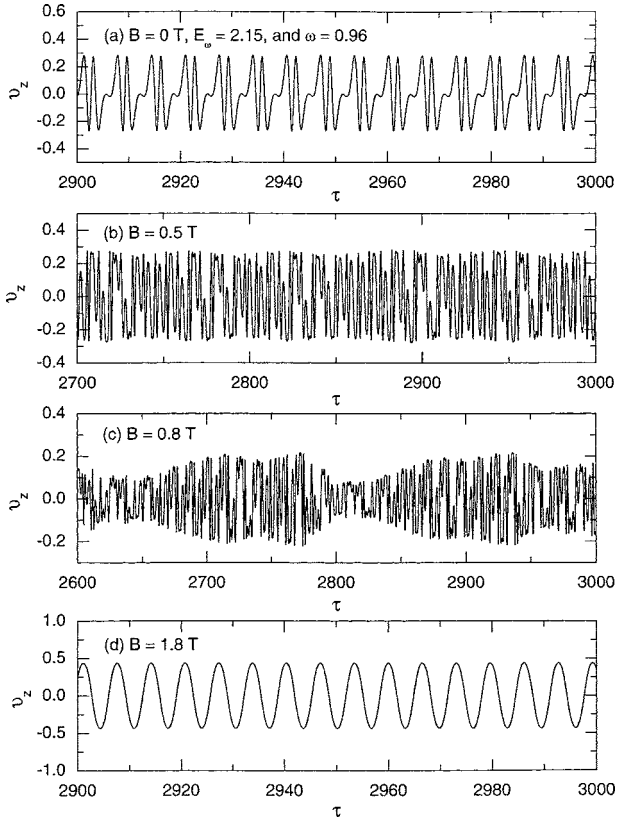

FIG. 1. Time-dependent average electron velocity v_z for a miniband superlattice of $\Delta=22$ meV at $T=4$ K, $\alpha=0.0001$, $E_\omega=2.15$, $\omega=0.96$, and different magnetic fields: $B=$(a) 0 T, (b) 0.5 T, (c) 0.8 T, and (d) 1.8 T, respectively.

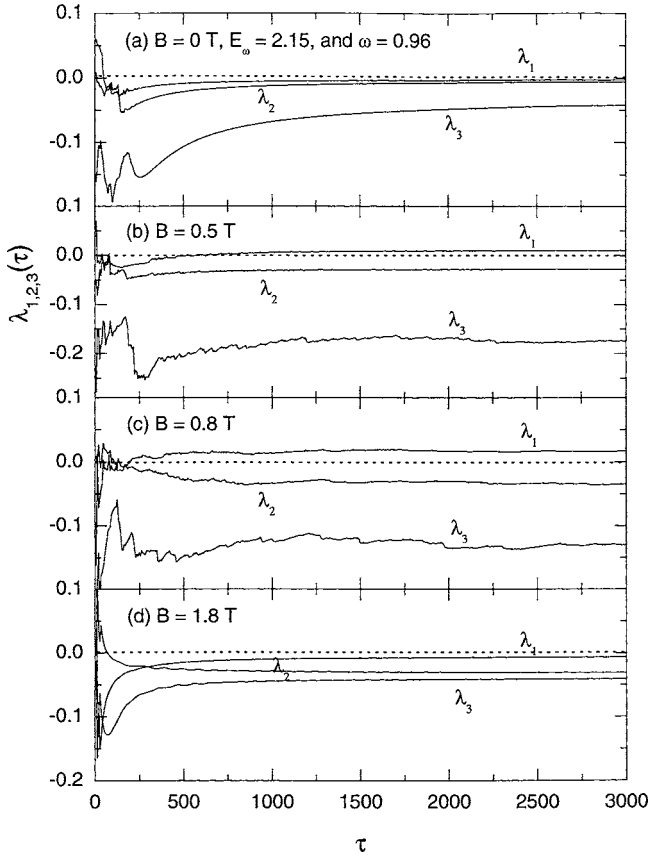

FIG. 2. Temporal convergences of the first three largest Lyapunov exponents for different magnetic fields: $B=$(a) 0 T, (b) 0.5 T, (c) 0.8 T, and (d) 1.8 T, respectively.

ternal electric field $E_\Omega \cos(\Omega t)$. The superlattice parameters are from the experiment of Ref. 5: $\Gamma_{Vy}=\Gamma_{Vz}=\Gamma_\varepsilon=10^{12}$ s^{-1}, $a=90$ Å, and $\Delta=22$ meV. The relaxation frequency of the external circuit is set to be $\alpha=0.0001$ and the lattice temperature is $T=4$ K. For the bulk density $N=1.0\times10^{14}$ cm^{-3}, the frequency $\omega_s\approx1.904\times10^{12}$ s^{-1}. We set the initial conditions as $v_y(0)=0$, $v_z(0)=0$, $w(0)=w_0$, and $E(0)=E_\omega$, which correspond to the electron in the initially unexcited states, to solve the Eqs. (9)–(12). Using the integrating-one-step Gill algorithm method incorporating adaptive step size and convergence checking with an accuracy of 10^{-6}, we get the numerical solutions of the superlattice system.

The normalized ac electric field amplitude E_ω can also be expressed by $E_\omega=\omega_B/\omega_s$, with $\omega_B=eaE_\Omega/\hbar$ the Bloch oscillation frequency. Thus the normalized electric field amplitude characterizes the relation between the Bloch oscillation frequency and electron plasma oscillation frequency. After applying the magnetic field, the electron's cyclotron frequency at the miniband bottom can be defined as $\omega_c=eB/\sqrt{m_0m^*}$ within the semiclassical approximation. The dimensionless magnetic field $\mathcal{B}=eB/(\omega_s\sqrt{m_0m^*})=\omega_c/\omega_s$ represents the relationship between the cyclotron frequency and electron plasma frequency. The Bloch frequency and cyclotron frequency are determined by the external electric field and magnetic field, respectively. It has been discussed in Ref. 31 that these oscillations do not hybridize but they can suppress one another. In the following sections, we will show that the competition between internal oscillations and the external electric field oscillation will lead to complicated chaotic dynamical characteristics.

III. TEMPORAL EVOLUTION OF AVERAGE ELECTRON VELOCITY IN MINIBAND SUPERLATTICES

In Eqs. (9)–(12) there are four independent variables: average electron velocities v_y and v_z, energy w, and electric field E, involving three control parameters: magnetic field $\mathcal{B}$, ac amplitude E_ω, and ac frequency ω. Since the average electron velocity v_z is the variable most directly related to experimental observable, we deal with the temporal evolution of v_z at different magnetic fields in this section. The parameters of the external electric field parallel to growth axis are fixed at $E_\omega=2.15$ and $\omega=0.96$ (corresponding to $E_\Omega=3.0\times10^5$ V/m and $\Omega=1.83\times10^{12}$ s^{-1}). We directly solve Eqs. (9)–(12) at four different magnetic fields and get the temporal solutions of v_z which are depicted in Fig. 1. It is found that different temporal behaviors of the miniband superlattice system show up when changing the magnetic field. For magnetic fields $B=0$ and 1.8 T (corresponding to $\mathcal{B}=0$ and 2.196, respectively), average velocity v_z displays regular oscillations which are shown in Figs. 1(a) and 1(d). These are the so-called "periodic" behavior, which means that the average velocity varies periodically with just the fundamental

frequency or its subharmonics of the external ac frequency.[24] In the periodic region, the system's solution enters a frequency-locking mode with the external controlling frequency. The temporal evolution of velocity v_z for $B=0.5$ and 0.8 T (corresponding to $\mathcal{B}=0.61$ and 0.976, respectively) are plotted in Figs. 1(b) and 1(c), respectively. The chaotic velocities vary erratically and appear to be very complex. In addition to the periodic and chaotic behaviors, there is another kind of behavior which is named "quasiperiodic."[18,24] The quasiperiodic is a type of very interesting dynamical motion. It can be basically thought of as a mixture of periodic motions of several different fundamental frequencies.[32]

Lyapunov exponents have been proven to be the most effective method to distinguish the periodic, quasiperiodic, and chaotic solutions. They are obtained from the average exponential rates of divergence or convergence of nearby orbits in phase space. For each set of parameters, the Lyapunov exponents vary with time and eventually converge to asymptotic values. For the chaotic solutions, the Lyapunov exponents contain at least one asymptotic value greater than zero. The system containing more than one positive Lyapunov exponent is considered to be a high-dimensional chaotic system. In our calculation, high-dimensional chaos is not observed. Generally, we use the largest Lyapunov exponent λ_1 to discriminate the three types of solutions. If the largest Lyapunov exponent λ_1 is positive, the solution is defined as chaotic. For periodic solutions the largest Lyapunov exponent λ_1 is negative, while for quasiperiodic solutions λ_1 is equal to zero. We have calculated the first three Lyapunov exponents λ_1, λ_2, and λ_3 with the standard method and computational programs described in Ref. 33. In the calculations, we use the time interval $\tau_m=mT_{\rm ac}$ (with $m=1,2,\ldots$, and $T_{\rm ac}=2\pi/\omega$ the driving period of the ac field) to average the Lyapunov exponents. The calculated temporal convergence of the first three Lyapunov exponents $\lambda_1(\tau)$, $\lambda_2(\tau)$, and $\lambda_3(\tau)$ for different magnetic fields are shown in Fig. 2, in which the maximal time delay is about $460T_{\rm ac}$. It can be seen from Fig. 2 that the asymptotic value of the largest Lyapunov exponents $\lambda_1(\tau)$ for the periodic cases $B=0$ and 1.8 T are less than zero, while those for the chaotic cases $B=0.5$ and 0.8 T are greater than zero, as they should be.

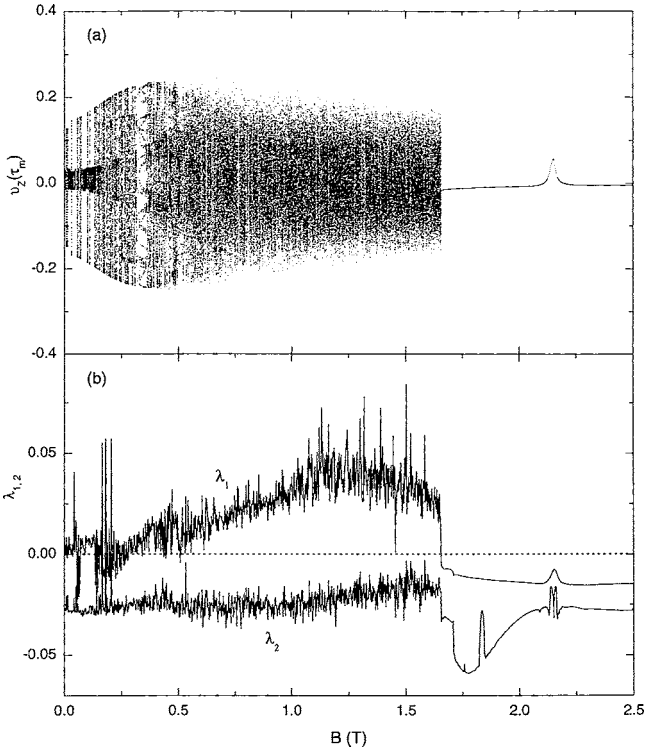

FIG. 3. (a) Poincaré bifurcation diagram of average electron velocity v_z and (b) the first two Lyapunov exponents for the superlattice system with the magnetic field B as the control parameter. (The external electric field $E_\omega=2.06$ and $\omega=0.89$.)

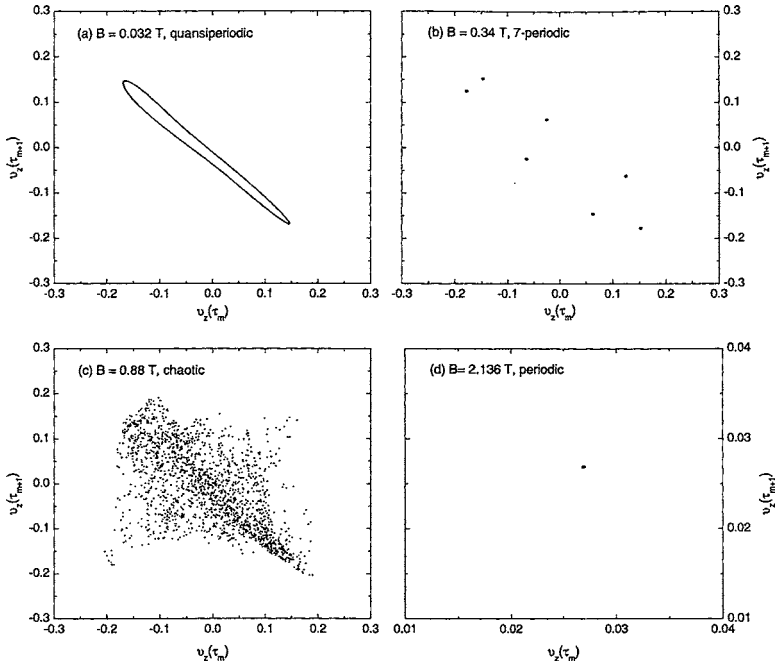

FIG. 4. First return map for average electron velocity v_m at different magnetic fields: $B=$(a) 0.032 T, (b) 0.34 T, (c) 0.88 T, and (d) 2.136 T, respectively.

IV. CHAOTIC DYNAMICS IN MINIBAND SUPERLATTICES WITH DIFFERENT CONTROL PARAMETERS

Now, we deal with the nonlinear dynamical characteristics of average velocity v_z in the miniband superlattice system at the presence of electric and magnetic fields. First, we select the magnetic field B as the control parameter while the parameters of the electric field are fixed at $E_\omega=2.06$ and $\omega=0.89$ (corresponding to $E_\Omega=2.87\times10^5$ V/m and $\Omega=1.69\times10^{12}$ s^{-1}). To clarify the periodic and aperiodic (quasiperiodic or chaotic) regions in the parameter space, we need the help of a Poincaré bifurcation diagram.[14,20,24] The Poincaré mapping is calculated using the techniques introduced in Ref. 14 and we adopt the average electron velocities $v_m=v(mT_{\rm ac})$ $(m=1,2,\ldots$ after the transients die out) as the Poincaré maps. The interesting bifurcation diagram is shown in Fig. 3(a) with the magnetic field changing from 0 to 2.5 T. In the mapping, the solutions for $B\geqslant1.656$ T become 1:1 frequency-locking. The periodic solutions also appear in the region of $B\in(0,1.656)$ where the mapping is full of a large number of points. The periodic windows are so small that it is difficult to distinguish the periodic solutions from the aperiodic ones from the mapping. In Fig. 3(b), we present the first two Lyapunov exponents λ_1 and λ_2 as functions of magnetic field B. With the help of Lyapunov expo-

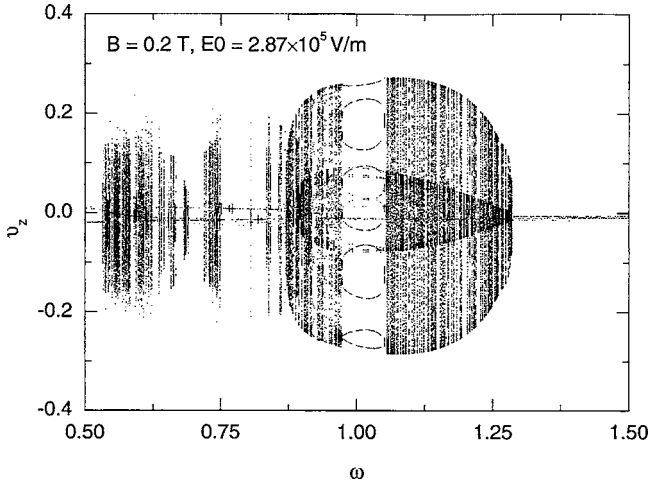

FIG. 5. Poincaré bifurcation diagram of average electron velocity v_z with ac frequency ω as the control parameter. (The ac amplitude $E_\omega=2.06$ and magnetic field $B=0.2$ T.)

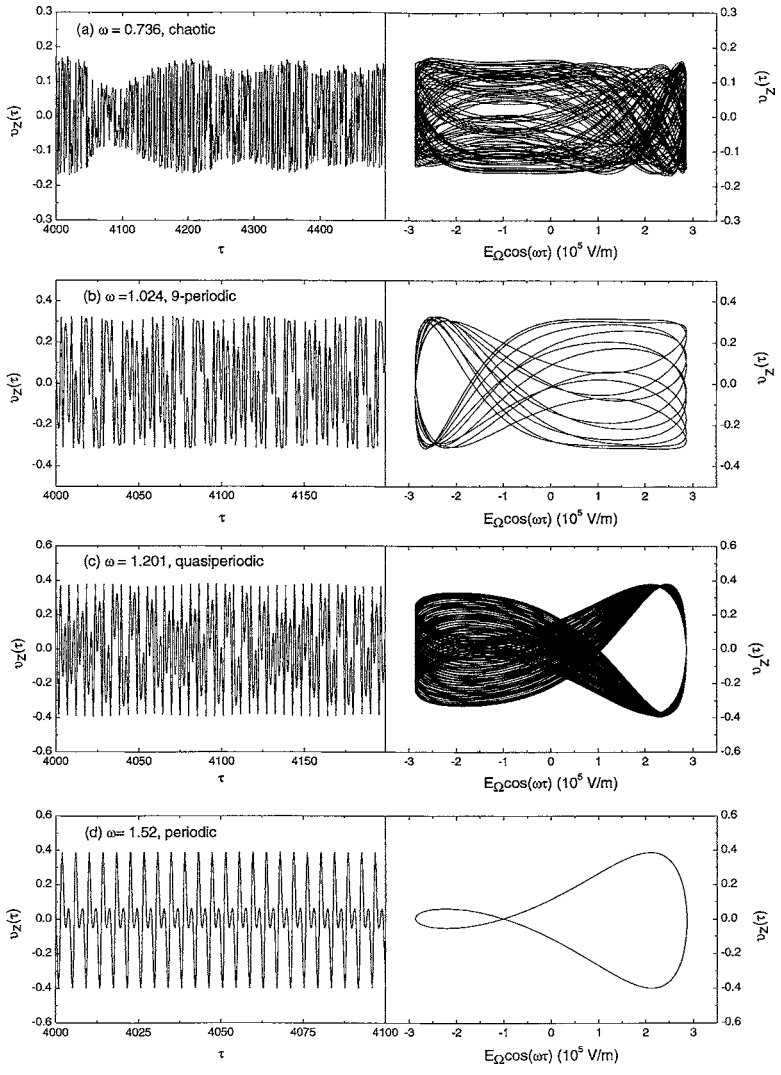

FIG. 6. Time-dependent average electron velocities $v(\tau)$ (left) and the corresponding velocity-field phase plots (right) for four specific ac frequencies: ω=(a) 0.736, (b) 1.024, (c) 1.201, and (d) 1.52, respectively.

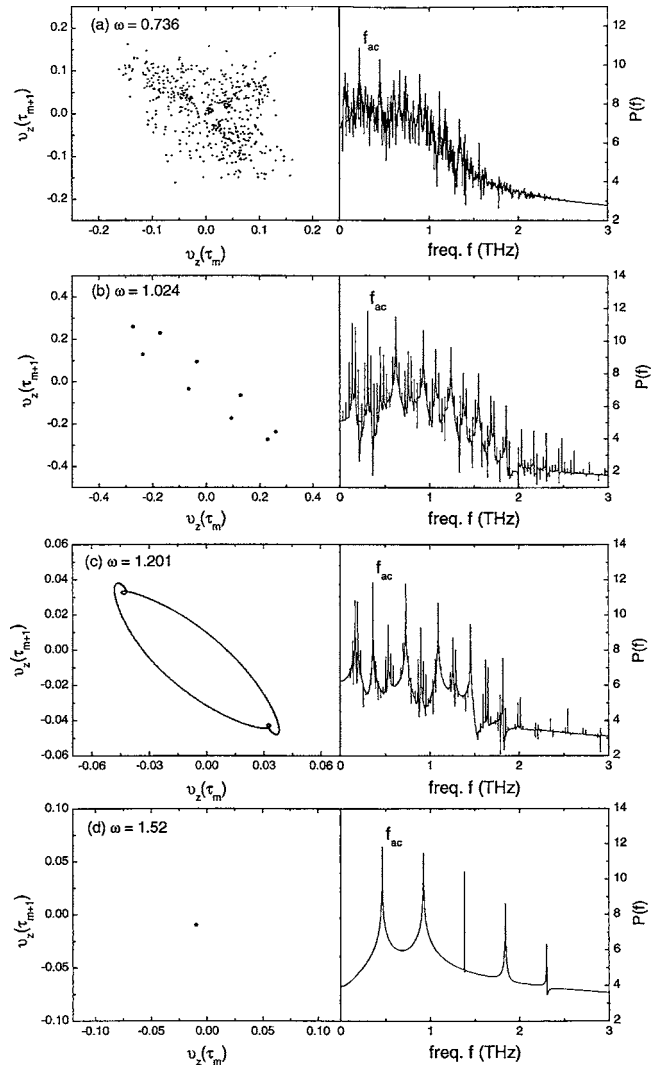

FIG. 7. First return maps (left) and power spectra (right) for the four specific ac frequencies as in Fig. 6.

nents, we can clarify the periodic ($\lambda_1<0$), quasiperiodic ($\lambda_1=0$), and chaotic ($\lambda_1>0$) solutions from the mapping. For $B\leqslant 0.508$ T, the periodic, quasiperiodic, and chaotic solutions appear and the transitions among them are disconnected and irregular. In the region of $B\in(0.508,1.656)$, the first Lyapunov exponent λ_1 for each magnetic field B is positive which indicates the appearance of chaotic states. The occurrence of different oscillation modes is due to the competition between the external electric fields and internal oscillation modes. For $B\geqslant 1.656$ T, the first two Lyapunov exponents are both negative and the periodic solution is obtained. The Bloch frequency and cyclotron frequency reflect the control of the electric field and magnetic field, respectively. It is found that the ratio of Bloch frequency and cyclotron frequency $\omega_B/\omega_c\approx 1$ for $E_\Omega=2.87\times 10^5$ V/m and $B=1.656$ T, i.e., the solution of average velocity $v_z(\tau)$ become 1:1 frequency-locking with the external ac frequency when $\omega_B/\omega_c\approx 1$. With the further increase of magnetic field, the electron is strongly restricted by the magnetic field and the average velocity is synchronized with the external electric field.

To have a deep insight into the different behaviors of the system, we use the first return map which is obtained by plotting v_{m+1} as a function of v_m (here m is large enough so that the transient states die out). The first return map can be a single point, a number of isolated points, or a closed smooth loop.[19] In Fig. 4 we plot the first return map for B =(a) 0.032, (b) 0.34, (c) 0.88, and (d) 2.136 T. The n separate points indicate that the solution is n-periodic [Figs. 4(b) and 4(d)]. The first return map for quasiperiodic solution is a closed smooth loop [Fig. 4(a)] while the one for chaotic solution contains many isolated points with varying density on different regions [Fig. 4(c)].

We have also studied the average electron velocity at different driving frequencies ω when fixing the ac amplitude E_ω and magnetic field B. In Fig. 5 we show the Poincaré bifurcation diagram with $E_\omega=2.06$ and $B=0.2$ T (corresponding to $\mathcal{B}=0.244$). The ac frequency ω changes from 0.5 to 1.5. From the mapping, the regions full of a large number of points indicate the appearance of aperiodic solutions, which can be easily distinguished from the periodic ones.[14] The Poincaré bifurcation diagram also indicates that the bifurcation scenario is quite complex, rather than a simple period-doubling cascade commonly appearing in nonlinear dynamical systems. The transition between periodic and aperiodic states changes discontinuously with the parameter ω. Even in the periodic region the bifurcation diagram can be discontinued, such as in the region of $\omega\in(0.75,0.835)$. As ω increases, the periodic and aperiodic solutions show up alternatively. For $\omega>1.287$, the solutions are 1:1 frequency-locking which indicates that the oscillation frequency of average velocity is synchronized with the driving frequency. It is noted that the average velocity v_m for the 1-periodic solution changes discontinuously with the increase of ac frequency ω.

Finally we have studied the behaviors of the average electron velocity using different chaos-detecting methods. We study in detail four specific cases of the ac frequencies: ω =(a) 0.736, (b) 1.024, (c) 1.201, and (d) 1.52, respectively. In Fig. 6, we depicted the time-dependent average electron velocity $v_z(\tau)$ (left) and the corresponding velocity-field phase plots (right) for the four ac frequencies. From the time-dependent evolution of average velocities $v_z(\tau)$, we can only clarify the periodic and aperiodic solutions. To discriminate the quasiperiodic from the chaotic solutions, we need the help of phase plot and first return map. Phase plots for the periodic solutions are quite simple with several closed loops [Figs. 6(b) and 6(d)], those for the quasiperiodic solutions are more complicated [Fig. 6(c)], while phase plots for the chaotic solutions become very much fold and irregular [Fig. 6(a)]. The first return maps for the four specific ac frequencies are shown in Fig. 7 (left). As we have described in the above paragraph, the resultant attractor for n-periodic solutions is just the n separate points [Figs. 7(b) and 7(d)], the one for the quasiperiodic solution is a closed smooth loop with a regular distribution of the points [Fig. 7(c)], while the chaotic attractor contains many isolated points with varying density of the points on different regions [Fig. 7(a)]. Power spectrum analysis is an additional effective method to detect chaos. Using the fast Fourier transform algorithm, we have

calculated the power spectra for the four specific ac frequencies which are shown in Fig. 7 (right). It is indicated that the power spectra for the n-periodic solutions [Figs. 7(b) and 7(d)] are simple and just have n peaks in the region of $f \in (0, f_{ac}]$ (here $f_{ac}=\Omega/2\pi=\omega\omega_s/2\pi$). These peaks correspond to the driving frequency f_{ac} and its harmonics. The power spectrum for the quasiperiodic solution [Fig. 7(c)] is relatively complex with few small peaks showing up near the main peaks, while the one for the chaotic solution [Fig. 7(a)] becomes very irregular with a large number of peaks.

V. CONCLUSIONS

We have theoretically studied the ballistic electron transport in GaAs-based superlattices driven by the THz electric field and constant magnetic field, based on the phenomenological balance equations. With the influence of magnetic field B, average electron velocity v_z displays very interesting nonlinear dynamical properties. With ac frequency ω and magnetic field B varying in the parameter space, it is found that the miniband superlattice system exhibits three types of time-dependent behaviors: periodic, quasiperiodic, and chaotic. For some parameters the solutions are chaotic and the bifurcation scenarios are very complex. In the present paper, the appearance of different nonlinear properties is contributed to the suppression of the internal oscillation mechanism and the competition between the external electric oscillation and internal oscillations. These nonlinear properties are carefully investigated using different chaos-detecting techniques including Poincaré bifurcation diagram, Lyapunov exponent, phase plot, first return map, and power spectrum.

ACKNOWLEDGMENTS

This work was supported by the National Fund for Distinguished Young Scholars of China (60425415), the major project of the National Science Foundation of China (10390162), the Special Funds for Major State Basic Research of China (G20000683), and the Shanghai Municipal Commission of Science and Technology (03JC14082).

*Electronic address: jccao@mail.sim.ac.cn

[1] L. Esaki and R. Tsu, IBM J. Res. Dev. **14**, 61 (1970).
[2] A. A. Ignatov, K. F. Renk, and E. P. Dodin, Phys. Rev. Lett. **70**, 1996 (1993).
[3] A. A. Ignatov, E. Schomburg, J. Grenzer, K. F. Renk, and E. P. Dodin, Z. Phys. B: Condens. Matter **98**, 187 (1995).
[4] A. A. Ignatov and A. P. Jauho, J. Appl. Phys. **85**, 3643 (1999).
[5] C. Rauch, G. Strasser, K. Unterrainer, W. Boxleitner, E. Gornic, and A. Waker, Phys. Rev. Lett. **81**, 3495 (1998).
[6] R. Aguado and G. Platero, Phys. Rev. Lett. **81**, 4971 (1998).
[7] E. Schomburg, A. A. Ignatov, J. Grenzer, K. F. Renk, D. G. Pavel'ev, Yu. Koschurinov, B. J. Melzer, S. Ivanov, S. Schaposchnikov, and P. S. Kop'ev, Appl. Phys. Lett. **68**, 1096 (1996).
[8] B. J. Keay, S. J. Allen, Jr., J. Galán, J. P. Kaminski, K. L. Campman, A. C. Gossard, U. Bhattacharya, and M. J. W. Rodwell, Phys. Rev. Lett. **75**, 4098 (1995).
[9] B. J. Keay, S. Zeuner, S. J. Allen, Jr., K. D. Maranowski, A. C. Gossard, U. Bhattacharya, and M. J. W. Rodwell, Phys. Rev. Lett. **75**, 4102 (1995).
[10] K. Unterrainer, B. J. Keay, M. C. Wanke, S. J. Allen, D. Leonard, G. Medeiros-Ribeiro, U. Bhattacharya, and M. J. W. Rodwell, Phys. Rev. Lett. **76**, 2973 (1996).
[11] F. Löser, M. M. Dignam, Yu. A. Kosevich, K. Köhler, and K. Leo, Phys. Rev. Lett. **85**, 4763 (2000).
[12] X. L. Lei, J. Appl. Phys. **82**, 718 (1997).
[13] O. M. Bulashenko and L. L. Bonilla, Phys. Rev. B **52**, 7849 (1995).
[14] O. M. Bulashenko, M. J. García, and L. L. Bonilla, Phys. Rev. B **53**, 10008 (1996).
[15] Y. Zhang, J. Kastrup, R. Klann, K. H. Ploog, and H. T. Grahn, Phys. Rev. Lett. **77**, 3001 (1996).
[16] K. J. Luo, H. T. Grahn, K. H. Ploog, and L. L. Bonilla, Phys. Rev. Lett. **81**, 1290 (1998).
[17] K. J. Luo, H. T. Grahn, S. W. Teitsworth, and K. H. Ploog, Phys. Rev. B **58**, 12613 (1998).
[18] D. Sánchez, G. Platero, and L. L. Bonilla, Phys. Rev. B **63**, 201306 (2001).
[19] O. M. Bulashenko, K. J. Luo, H. T. Grahn, K. H. Ploog, and L. L. Bonilla, Phys. Rev. B **60**, 5694 (1999).
[20] J. C. Cao and X. L. Lei, Phys. Rev. B **60**, 1871 (1999).
[21] K. N. Alekseev, G. P. Berman, D. K. Campbell, E. H. Cannon, and M. C. Cargo, Phys. Rev. B **54**, 10625 (1996).
[22] K. N. Alekseev, E. H. Cannon, J. C. McKinney, F. V. Kusmartsev, and D. K. Campbell, Phys. Rev. Lett. **80**, 2669 (1998).
[23] Yu. A. Romanov and Yu. Yu. Romanova, JETP **91**, 1033 (2000).
[24] J. C. Cao, H. C. Liu, and X. L. Lei, Phys. Rev. B **61**, 5546 (2000).
[25] J. C. Cao, Phys. Rev. Lett. **91**, 237401 (2003).
[26] B. Q. Sun, J. N. Wang, W. K. Ge, Y. Q. Wang, D. S. Jiang, H. J. Zhu, H. L. Wang, Y. M. Deng, and S. L. Feng, Phys. Rev. B **60**, 8866 (1999).
[27] E. H. Cannon, F. V. Kusmartsev, K. N. Alekseev, and D. K. Campbell, Phys. Rev. Lett. **85**, 1302 (2000).
[28] A. A. Krokhin, T. M. Fromhold, A. E. Belyaev, H. M. Murphy, L. Eaves, D. Sherwood, P. C. Main, and M. Henini, Phys. Rev. B **63**, 195323 (2001).
[29] T. Schmidt, A. G. M. Jansen, R. J. Haug, K. v. Klitzing, and K. Eberl, Phys. Rev. Lett. **81**, 3928 (1998).
[30] T. M. Fromhold, A. A. Krokhin, C. R. Tench, S. Bujkiewicz, P. B. Wilkinson, F. W. Sheard, and L. Eaves, Phys. Rev. Lett. **87**, 046803 (2001).
[31] Yu. A. Kosevich, Phys. Rev. B **63**, 205313 (2001).
[32] E. Ott, *Chaos in Dynamical Systems* (Cambridge University Press, Cambridge, 1993).
[33] A. Wolf, J. B. Swift, H. L. Swinney, and J. A. Vastano, Physica D **16**, 285 (1985).